J Electr Eng Technol.2018; 13(5): 2004-2010
http://doi.org/10.5370/JEET.2018.13.5.2004

ISSN(Print) 1975-0102
ISSN(Online) 2093-7423

Active GNSS Antenna Implemented with Two-Stage LNA on High Permittivity Substrate

Jong-Gyu Go* and Jae-Young Chung†

Abstract – We propose a small active antenna to receive Global Navigation Satellite System (GNSS) signals, i.e., Global Positioning System (GPS) L1 (1,575MHz) and Russian Global Navigation Satellite System (GLONASS) L1 (1,600 MHz) signals. A two-stage low-noise amplifier (LNA) with more than 27 dB gain is implemented in the bottom layer of a three-layer antenna package. In addition, a hybrid coupler is used to combine signals from pair of proximately coupled orthogonal feeds with 90° phase difference to achieve the circular polarization (CP) characteristic. Three layers of high permittivity (ε_r = 10) substrates are stacked and effectively integrated to have a small dimension of 64 mm×64 mm×7.42 mm (including both circuit and antenna). The reflection coefficient of the fabricated antenna at the target frequency is below −10 dB, the measured antenna gain is above 26 dBic and the measured noise figure is less than 1.4 dB.

Keywords: Active antenna, Axial ratio, Circularly polarization, Global navigation satellite system, Patch antenna.

1. Introduction

With the evolution of unmanned aerial vehicle systems (UAVs) the importance of location services based on the global navigation satellite system (GNSS) has increased. GNSS signals are transmitted at a distance of 20,000 km or more from the Earth; thus, they are susceptible to noise as the reception sensitivity is reduced [1-2]. Therefore, to realize a high-quality location service, the reception sensitivity degradation on the receiving end must be compensated.

To increase the reception sensitivity, an active antenna system combining a low-noise amplifier (LNA) and circular polarization (CP) antenna is adopted [3-6]. With the properly designed LNA, the received signal gain can be increased while minimizing additional noise, improving the reception sensitivity of the system. However, the size and complexity of the antenna package increases since an additional printed circuit board (PCB) layer is required to implement the LNA circuitry and several vias need to be placed to connect different PCB layers [7-8]. The latter also limits the choice of PCB type and thickness that can be used in the antenna design.

In this paper, we propose an LNA integrated active antenna design using a high permittivity multi-layer substrate for miniaturization. The use of high permittivity substrate is known to reduce the antenna size by reducing the effective wavelength and resonant frequency with the expense of lower antenna gain [9-10]. The antenna package consists of three layers such as radiating patch, feed and LNA circuitry, and they are all sharing the same ground plane. To avoid using vias, a pair of microstrip lines along the substrate wall is designed to connect a pair of feed lines. These orthogonal feeds are proximately coupled to the radiator on the top layer, therefore no direct connection (i.e., via) is needed [11-12].

We note that this work is an extension of preliminary results reported in a conference paper [13]. Antenna optimization processes are described in details, and improved measurement data of passive/active radiation patterns and axial ratio are included. The measured data shows that the designed active antenna has a superior S_{11} < -10 dB bandwidth from 1550-1640 MHz, the axial ratio less than 1.1 dB throughout the bandwidth, and the antenna gains more than 28 dB at GPS L1 (1,575 MHz) and GLONASS L1 (1,600 MHz) bands. In Section II, the antenna configuration is presented, and then Section III describes the design process for each layer based on electromagnetic and circuit simulators. In Section IV, the measurement results of the fabricated prototype are presented.

2. Antenna Configuration

Fig. 1 shows the proposed antenna structure. The total size of the integrated antenna is $64 \times 64 \times 7.42$ mm^3 and it is fabricated using low-loss high-permittivity substrate Taconic CER-10 with the relative permittivity of ε_r = 10, loss tangent of tan δ = 0.0035, and thickness of 2.54 mm for a single layer. As shown in Fig. 1(a), the antenna

† Corresponding Author: Dept. of Electrical and Information Engineering, Seoul Nat'l Univ. of Science and Technology, Korea. (jychung@seoultech.ac.kr)
* Dept. of Electrical and Information Engineering, Seoul Nat'l Univ. of Science and Technology, Korea. (jonggyu0129@gmail.com)
Received: January 16, 2018; Accepted: February 6, 2018

Copyright ⓒ The Korean Institute of Electrical Engineers
This is an Open-Access article distributed under the terms of the Creative Commons Attribution Non-Commercial License (http://creativecommons.org/licenses/by-nc/3.0/) which permits unrestricted non-commercial use, distribution, and reproduction in any medium, provided the original work is properly cited.

consists of three layers, i.e., patch, feed, and circuit layers. The patch layer is not directly connected to the feed layer, but is coupled via the two orthogonal proximate feeding structures. The feed and circuit layers are connected by a microstrip line extending along the wall side.

Fig. 1 (b) and (c) show detailed views of top and bottom of the circuit layer. The top of the circuit layer is the ground plane and the $S_1 \times S_2$ slot is used to avoid direct contact between the wall microstrip line and ground plane. The lower part includes a surface acoustic wave (SAW) band-pass filter to remove unwanted bands, a hybrid coupler with a 90° phase difference, and a two-stage LNA circuit. The three layers are tightly bound using polyvinyl chloride (PVC) bolts and nuts with minimized propagation effects. They were also included in the simulation model. Note that a 3D full-wave electromagnetic simulation tool (Ansys HFSS) and circuit simulation tool (National Instrument AWR) were used for antenna geometry and circuit layout optimizations. Table 1 lists the optimized antenna parameters.

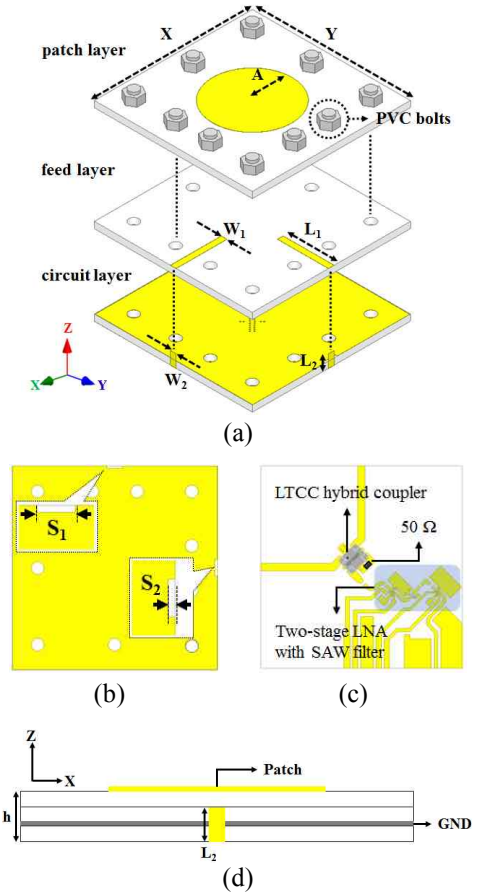

Fig. 1. Proposed antenna geometry: (a) perspective view, (b) top and (c) bottom views of 3rd layer, (d) side view

Table 1. Optimized Antenna Parameters (Defined in Fig. 1)

Parameter	Value (mm)	Parameter	Value (mm)
X	64	W_2	2.3
Y	64	L_2	2.54
A	16	S_1	5
W_1	2.3	S_2	2
L_1	20	h	7.62

3. Antenna Design and Optimization

3.1 Antenna radiator and feeding

The well-known patch antenna design equations [14] are used to determine the radius of the radiating circular patch [A in Fig. 1(a)] operating at the frequency of interest, GPS L1 (1,575 MHz) and GLONASS L1 (1,600 MHz) bands:

$$A = \frac{F}{\left\{1+\frac{2h}{\pi\varepsilon_r}\left[\frac{\pi F}{2h}\right]+1.7726\right\}^{1/2}} \quad (1)$$

$$F = \frac{8.791\times10^9}{f_r} \quad (2)$$

where f_r is the resonant frequency, ε_r and h are the relative permittivity and thickness of the substrate, respectively. The width of the coupled feed line (W_1 in Fig. 1) is determined to have 50 Ω at f_r = 1,587 MHz, which corresponds to the center frequency of GPS L1 (1,575 MHz) and GLONASS L1 (1,600 MHz). We note that the reflection coefficient (S_{11}) of the antenna was affected by the change of W_1 (and/or W_2) for the passive antenna but hardly changed the S_{11} of the active antenna. The two orthogonal coupled feeds are connected to the hybrid coupler RCP1500Q03 [15] in the circuit layer. The hybrid coupler is responsible for introducing 90° phase difference between the signals from each coupled feed to exploit CP characteristic.

Fig. 2 shows a diagram of the top layer patch and second layer coupled feed structures of the proposed antenna. Once the resonant frequency of the patch antenna is determined by A, the impedance matching condition can be adjusted by the overlapping length S between the coupled

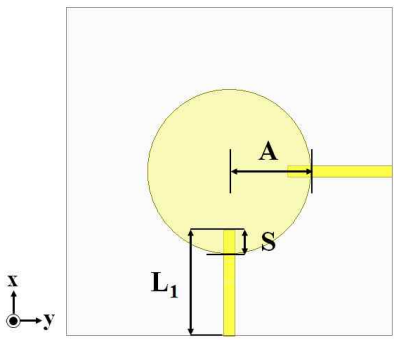

Fig. 2. Intersection length between antenna radiator and coupled feed line

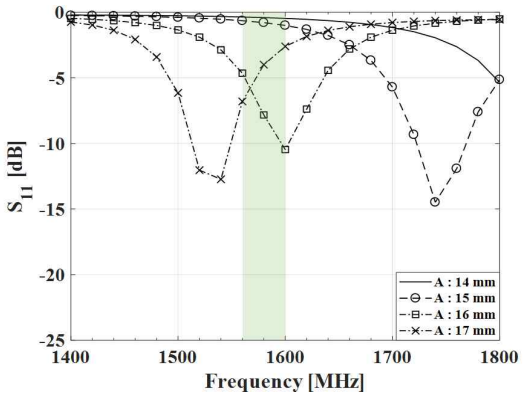

(a)

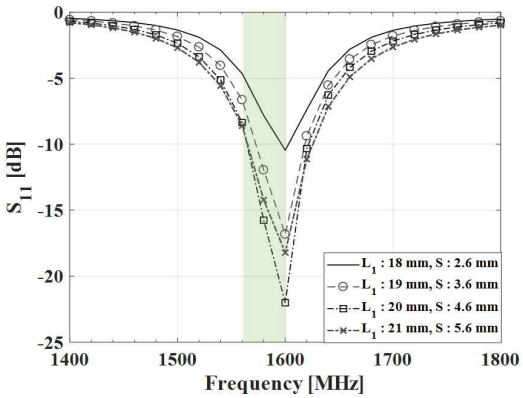

(b)

Fig. 3. Parametric study of S_{11}: (a) S_{11} with fixed L_1 = 21 mm and varied A, (b) S_{11} with fixed A = 16 mm and varied L_1 and S

feed and radiator.

Fig. 3(a) shows parametric simulations of the changes in the antenna resonant frequency (f_r) by varying A, the patch radius. f_r is determined by the frequency where the reflection coefficient (S_{11}) is minimum. Obviously, f_r shifts to the lower frequency for larger A. For A = 16 mm, f_r = 1,600 MHz close to the band of interest. However, the minimum S_{11} is only -10 dB. Thus, further optimization is required to reduce S_{11} to secure more impedance matching bandwidth.

This can be done by controlling the overlapping length S. Fig. 3(b) shows parametric simulations of the changes in the reflection coefficient (S_{11}) by varying L_1 and S. As can be seen, the S_{11} reduces as S is increases from 2.6 to 4.6 mm, implying the matching condition improves as the electromagnetic field coupling enhances. However, the S_{11} increases as the electromagnetic field is over-coupled by increasing S from 4.6 to 5.6 mm. Therefore, it is important to find the optimal coupled feed length by considering the under- and over-coupling transitions [16].

3.2 LNA circuitry

A two-stage LNA circuit design strategy is employed to deliver more than 30 dB gain and less than 1.5 dB noise figure (NF) at GPS L1 and GLONASS L1 bands. Fig. 4(a) and (b) show a block diagram of LNA circuit and its corresponding layout at the antenna's bottom layer. The LNA used is NXP BGU8019 whose gain is 18.5 dB in the frequency band from 1,500 MHz to 1,650 MHz. Thus theoretically, 37 dB gain can be carried out by cascading them in two stages.

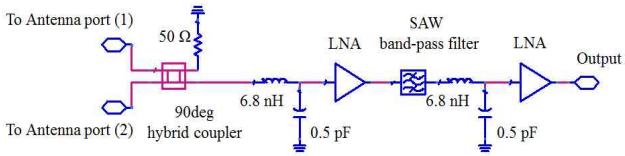

(a)

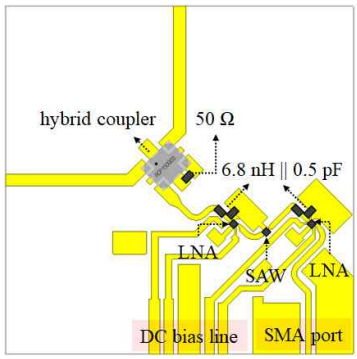

(b)

Fig. 4. (a) Block Diagram and (b) PCB layout of the circuit layer

A SAW bandpass filter (TDK B4327) with 3dB insertion loss is placed between the cascade connections of the two LNAs to prevent signal interference in unwanted bands. The LNA input is connected to a hybrid coupler with another 3dB insertion loss to combine the signals from two orthogonal feeds with 90° phase difference. Matching networks are implemented in between each component and then optimized using NI AWR circuit simulator to have maximum gain in the target frequency band.

4. Antenna Fabrication and Measurement

Two types of antennas were fabricated for the validation experiment: a passive antenna with no LNA circuit and an active antenna including the LNA circuit. Fig. 5(a) and (b) show pictures of the fabricated antenna (top side) and LNA circuit (bottom side), respectively.

Firstly, the gain and NF of two-stage LNA circuitry were measured using a vector network analyzer (VNA, Agilent N9913A), noise source (Agilent 346B), and spectrum analyzer (R&S FSW). 3.5 mm subminiature version A (SMA) connectors were mounted on one of the inputs of hybrid coupler and the output of LNA for the measurement. Fig. 6(a) and (b) show simulation and measurement results

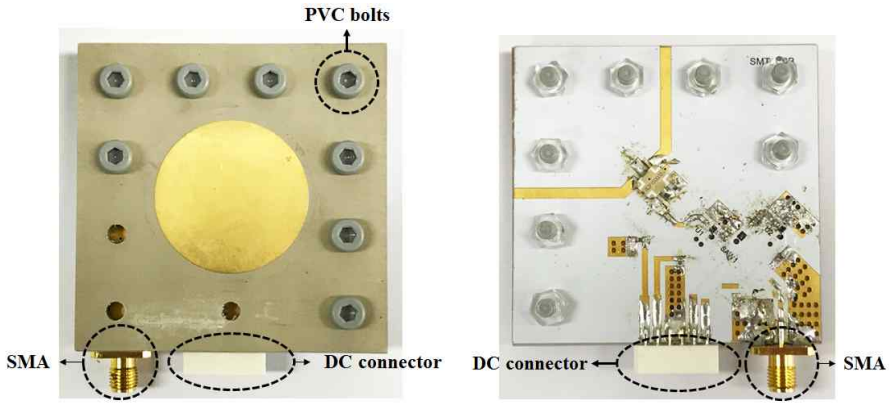

(a) (b)

Fig. 5. Pictures of the fabricated antenna: (a) top and (b) bottom

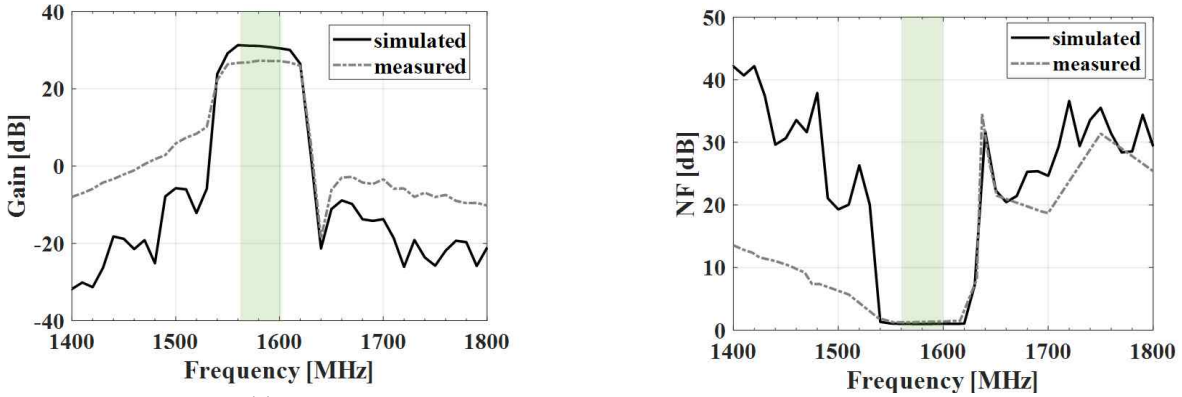

(a) (b)

Fig. 6. Comparison of simulated and measured results of the LNA circuit: (a) gain and (b) noise figure

Table 2. Measurement and simulation results for LNA circuit

Parameters	GPS L1 (1,575 MHz)	GLONASS L1 (1,600 MHz)
Simulated gain	30.85 dB	30.42 dB
Measured gain	27.82 dB	27.2 dB
Simulated NF	0.99 dB	1.01 dB
Measured NF	1.28 dB	1.38 dB

for the designed two-stage LNA. In these figures, the frequency range incorporating the GPS L1 and GLONASS L1 bands is shaded. We note that the electromagnetic-circuit co-simulation data were obtained using National Instrument AWR ver.12 software considering the same layout as the actual circuitry depicted in Fig. 4.

Table 2 summarize the simulation and measurement results at each band. The simulated gain and NF are around 30 dB and 1 dB, respectively, while the measured gain and NF are around 27 dB and 1.3dB, which are degraded from the simulation, possibly due to additional losses from the matching circuits and fabrication errors.

Next, S_{11} of the passive and active antennas were measured and compared with the simulation results. To

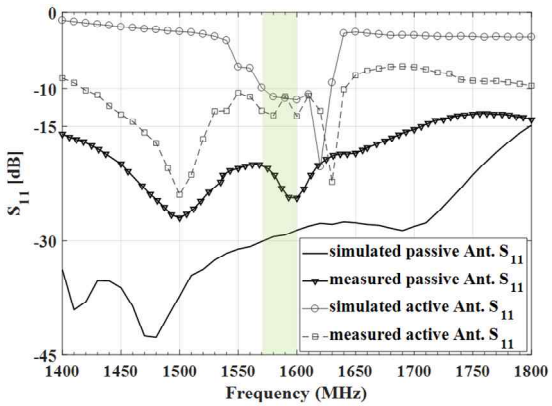

Fig. 7. Simulated and measured reflection coefficients of passive and active antennas

measure S_{11} of the passive antenna, the VNA was connected to a hybrid coupler port while the other was terminated with a 50-ohm load. On the other hand, S_{11} of the active antenna was measured by connecting the VNA to the LNA output.

Fig. 7 shows the measured S_{11} together with the simulation results. As can be observed, S_{11} of the passive

antenna is less –14 dB for the observed frequency range (1,400-1,800 MHz), including the shaded GPS L1 and GLONASS L1 bands. Note that the broadband characteristic of the passive antenna is due to the broadband matching performance of the hybrid coupler [17-18]. The simulated S11 is much lower than the measured results not only in the target frequency band but throughout the whole observation frequency range. This may come from fabrication errors such as unexpected gaps or misalignments between the layers, losses and mismatches due to soldering, material imperfection, etc. Also for the active antenna's S_{11}, errors exist between the simulated and measured data, however they have good agreements in the LNA operation bands and are below –10 dB.

Finally, the radiation characteristics of passive and active antennas were measured. To obtain the far-field radiation characteristics, the measurements were performed in an anechoic chamber. Fig. 8(a) and (b) show the measurement setups of the passive and active antennas. As shown in Fig. 9(b), DC biasing for the LNA circuit was incorporated in the measurement by mounting a battery-based power supply circuit on the scanning jig.

Fig. 9(a) and (b) show the measured far-field-radiation patterns at the center frequencies of the GPS L1 (1,575 MHZ) and GLONASS L1 (1,600 MHz) bands for the passive antenna. The patterns were measured along the xz-plane (See the coordinate convention in Fig. 1(a)). We note that the patterns along the yz-plane were not measured since the simulated radiation patterns exhibited symmetry in the xz- and yz-planes due to the geometrical symmetry of the antenna. Each plot contains right-handed (RHCP) and left-handed (LHCP) CP components. The passive antenna exhibited RHCP gains of 3.69 and 2.84 dBic for the GPS L1 and GLONASS L1 frequency bands, respectively. Fig. 10(a) and (b) show far-field radiation patterns of the active antenna incorporating the LNA circuit.

The measured RHCP gains in the GPS L1 and GLONASS L1 bands for the active antenna were 28.03 and 26.96 dBic, respectively. It is apparent that the gain of the active antenna is 24 dB higher than that of the passive antenna.

Fig. 11 shows the measured axial ratio (AR) characteristics of the passive and active antennas. Both the passive and active antennas exhibited AR < 3 dB in the observed frequency range of 1,500–1,650 MHz, which incorporates the GPS L1 and GLONASS L1 bands. The AR measurement results indicate that both the proposed passive and active antennas satisfy the AR characteristic requirement for GNSS signal reception, i.e., they are less than 3 dB. The AR characteristics of the passive antenna were 1.7 and 1.39 dB for GPS L1 and GLONASS L1, respectively. The AR characteristics of the active antenna were even lower, marking at 1.06 and 0.65 dB for the GPS L1 and GLONASS L1 bands, respectively. It has been

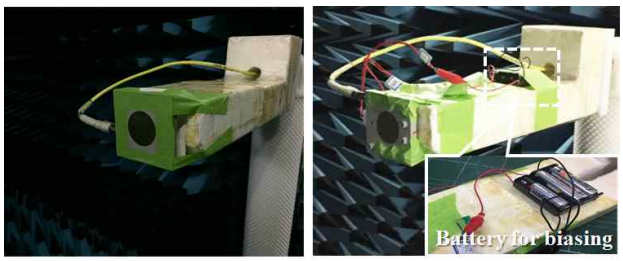

(a) (b)

Fig. 8. Antenna mounted on anechoic-chamber jig for (a) passive and (b) active antennas

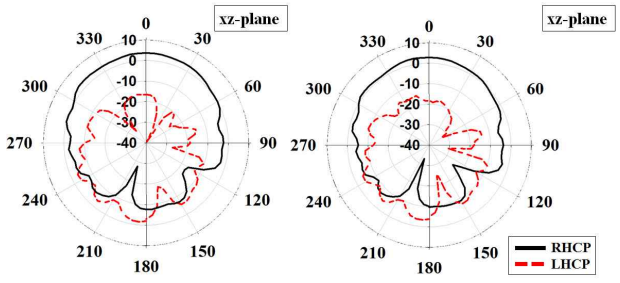

(a) (b)

Fig. 9. Far-field radiation patterns of passive antenna at (a) 1,575 and (b) 1,600 MHz

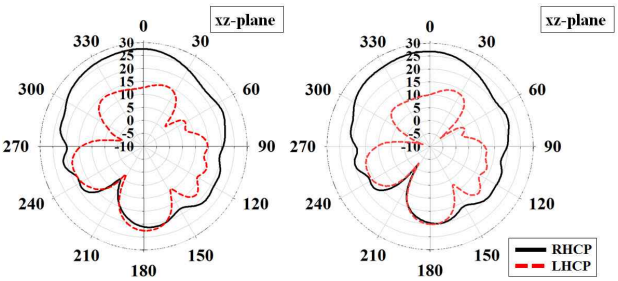

(a) (b)

Fig. 10. Far-field radiation patterns of active antenna at (a) 1,575 and (b) 1,600 MHz

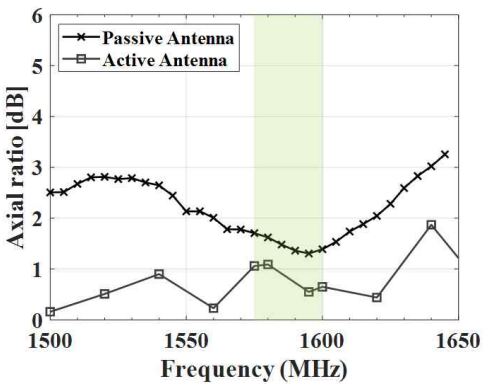

Fig. 11. Measured axial ratio of passive and active antennas

reported that high-dielectric substrates can be used to limit the field inside the substrate, yielding wide-band AR performance [9, 10]. Furthermore, the LNA circuitry including hybrid and saw filter promotes a better AR performance by increasing the difference between the RHCP and LHCP gains [4, 17].

5. Conclusion

In this paper, we proposed a two-stage LNA integrated CP antenna that operates in the GPS L1 (1,575 MHz) and GLONASS L1 (1,600 MHz) bands. The antenna consists of patch, feed, and circuit layers and is fabricated using a high permittivity substrate to facilitate miniaturization and to provide wide AR characteristics. The antenna circuit layer includes a two-stage LNA circuit to simultaneously provide high gain and low NF. In addition, the LNA circuitry includes a hybrid coupler to realize CP characteristics and a SAW band-pass filter to eliminate signal interference. The antenna circuit layer is mounted on the back of the ground plane shared by the antenna feeds which does not require additional space and complicated vias for implementation. Both the passive and active antennas examined in experiment had dimensions of $64 \times 64 \times 7.42$ mm^3.

The measured gains of the active antenna were 28.03 and 26.96 dBic for the GPS L1 and GLONASS L1 bands, respectively. In addition, based on the measured AR characteristics (> 1.7 dB), the proposed active antenna is expected to be applicable to various GNSS systems.

Acknowledgements

This work has been supported by the Future Combat System Network Technology Research Center program of Defense Acquisition Administration and Agency for Defense Development. (UD166070BD)

References

[1] K. Y. Kim, "Analysis of anti-jamming techniques for satellite navigation systems," *J. Korean Inst. Commun. Inf. Sci*., vol. 38, pp. 1216-1227, 2013.

[2] G. Byun, J. C. Hyun, S. M. Seo, H. Choo, "Optimum Array Configuration to Improve Null Steering Time for Mobile CRPA Systems," *J. Electromagn. Eng. Sci*., vol. 16, pp. 74-79, 2016.

[3] A. Friedrich, L. Berkelmann, T. Martinelli, B. Geck, O. Klemp, I. Kriebitzsch, "An active three-dimensional GPS patch antenna using MID-technology," *In proc. 2015 EuRAD*, 2015, pp. 373-376.

[4] Z. Wang, H. Liu, S. J. Fang, Y. Cao, "A low-cost dual-wideband active GNSS antenna with low-angle multipath mitigation for vehicle applications," *Prog. Electromagn. Res*., vol. 144, pp. 281-289, 2014.

[5] L. R. Kuo, W. J. Liao, H. T. Chou, "An Active Patch Antenna with Embedded LNA Module," *In Proc. IEEE-ISAP*, 2006, pp. 3639-3642.

[6] T. Fukusako, "Broadband Characterization of Circularly Polarized Waveguide Antennas Using L-Shaped Probe," *J. Electromagn. Eng. Sci*., vol. 17, pp. 1-8, 2017.

[7] J. H. Kim, M. S. Kim, J. S. Kim, S. B. Son, Y. B. Kim, "A Single Layer Multi Band Microstrip Patch Antenna for GPS L1/L2, GLONASS Receiver Applications," *J. Korea Inst. Electromagnet. Eng. Sci*., vol. 22, no. 10, pp. 990-998, 2011.

[8] Y. Q. Zhang, X. Li, L. Yang, S. X. Gong "Dual-band circularly polarized antenna with low wide-angle axial-ratio for tri-band GPS applications," *Prog. Electromagn. Res. C*, vol. 32, pp. 167-179, 2012.

[9] K. Y. Lam, K. M. Luk, K. F. Lee, H. Wong, K. B. Ng, "Small circularly polarized U-slot wideband patch antenna," *IEEE Antennas and Wireless Propagat., Lett*., vol. 10, pp. 87-90, 2011.

[10] K. B. Ng, C. H. Chan, K. M. Luk, "Low-cost vertical patch antenna with wide axial-ratio beam-width for handheld satellite communications terminals," *IEEE Trans. Antennas Propagat.*, vol. 63, no. 4, pp. 1417-1424, 2015.

[11] A. Dierck, H. Rogier, F. Declercq, "A wearable active antenna for global positioning system and satellite phone," *IEEE Trans. Antennas Propagat*., vol. 61, no. 2, pp. 532-538, 2013.

[12] N. Pham, J. Y. Chung, B. Lee, "A proximity-fed antenna for dual-band GPS receiver," *Prog. Electromagn. Res. C*, vol. 61, pp. 1-8, 2016.

[13] J. G. Go, J. Y. Chung, "A compact LNA integrated antenna for global navigation satellite systems," *In proc. IEEE-RFIT*, 2017, pp. 229-231.

[14] C. A. Balanis, "Antenna theory: analysis and design. New York," New Yokr: Wiley, 2005.

[15] RN2 Technologies, "LTCC 3dB Hybrid Coupler," RCP1500Q03 datasheet, Dec. 2012.

[16] H. Iwasaki, "A circularly polarized small-size microstrip antenna with a cross slot," *IEEE Trans. on Antennas Propagat*., vol. 44, no. 10, pp. 1399-1401, 1996.

[17] S. J. Jeong, K. C. Hwang, D. I. Hwang, "Compact circularly polarized antenna with a capacitive feed for GPS/GLONASS applications," *ETRI J*., vol. 34, no. 5, pp. 767-770, 2012.

[18] K. W. Khoo, Y. X. Guo, L. C. Ong "Wideband circularly polarized dielectric resonator antenna, *IEEE Trans. Antennas and Propagat*., vol. 55, no. 7, pp. 1929-1932, 2007.

[19] M. Chen, C. C. Chen, "A compact dual-band GPS antenna design," *IEEE Antennas and Wireless*

Propagat., Lett., vol. 12, pp. 245-248, 2013.
[20] L. S. Pereira, R. L. Farias, C. Lucatel, M. V. Heckler, A. F. T. Salazar, "Annular slot antenna for high-precision GPS applications," *In proc. IEEE-IMOC*, 2013, pp. 1-5.

Jong-Gyu Go received a B.S. degree from the Dept. of Information and Communication Eng., Dongyang Mirae University, Korea, in 2016, and an M.S. degree from the Dept. of Electrical and Information Eng., SeoulTech, Korea, in 2018. He is currently an RF engineer in Wisol, Korea. His research interests include RF circuit design, and Antenna design.

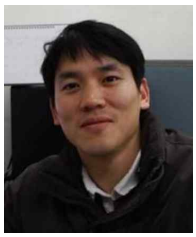

Jae-Young Chung received a B.S. degree from Yonsei University, Korea, in 2002, and an M.S. degree and Ph.D. from the Ohio State University, United States, in 2007 and 2010, respectively; all degrees were in electrical engineering. From 2002 to 2004, he was with Motorola Korea as an RF engineer. From 2010 to 2012, he worked at Samsung Electronics, Korea, as an antenna engineer. He is currently an Assistant Professor with the Department of Electrical and Information Engineering, Seoul National University of Science and Technology, Korea. His research interests include electromagnetic measurement and antenna design.